Geomechanics and Engineering, *Vol. 18, No. 2 (2019) 111-119*
DOI: https://doi.org/10.12989/gae.2019.18.2.111

Influence of explosives distribution on coal fragmentation in top-coal caving mining

Fei Liu*[1,2], Jhon Silva[3], Shengli Yang**[1,2], Huayong Lv[1,2] and Jinwang Zhang[1,2]

[1]School of Energy and Mining Engineering, China University of Mining & Technology, Beijing 100083, China
[2]Coal Industry Engineering Research Center of Top-Coal Caving Mining, Beijing 100083, China
[3]Department of Mining Engineering, University of Kentucky, Lexington, KY, 40506, U.S.A.

(Received April 1, 2019, Revised May 3, 2019, Accepted May 8, 2019)

Abstract. Due to certain geological characteristics (high thickness, rocky properties), some underground coal mines require the use of explosives. This paper explores the effects of fragmentation of different decks detonated simultaneously in a single borehole with the use of numerical analysis. ANSYS/LS-DYNA code was used for the implementation of the models. The models include an erosion criterion to simulate the cracks generated by the explosion. As expected, the near-borehole area was damaged by compression stresses, while far zones and the free surface of the boundary were subjected to tensile damage. With the increase of the number of decks in the borehole, different changes in the fracture pattern were observed, and the superposition effects of the stress wave became evident, affecting the fragmentation results. The superposition effect is more evident in close distances to the borehole, and its effect attenuates when the distance to the borehole increase.

Keywords: distributed charges; coal blasting; tensile damage; explosion cracks

1. Introduction

Due to particular geological conditions, some coalfields require the use of non-conventional mining methods elsewhere such as underground coal caving (Tien *et al.* 2017). The most popular excavation method for the mining of thick deposits is the longwall top coal caving (LTCC) method. Fig. 1, adapted from Xu (Xu 2004) shows the typical arrangement for the LTCC mining method.

There are many parameters influencing the cavability of the coal among others (Vakili *et al.* 2010, Alehossein and Poulsen 2010): a) Coal seam rock and rock mass properties; b) surrounding rock and rock mass characteristics; c) stress conditions and d) mining layout.

In general, one important aspect to develop a safe coal caving operation is to provide pre-fractured coal as a rock mass surrounding the caved zone (see Fig. 1). Having a pre-fractured coal-rock mass around the caved area will increase the cavability of the coal and will avoid stress concentrations that can be dangerous if combined with the brittle behavior of the coal (Sampath *et al.* 2017). The combination of brittle behavior and stress concentrations can generate a dangerous instantaneous release of energy that can be very difficult to control for the mining operation (Gasparotto *et al.* 2018, Li *et al.* 2019, Ozacar 2018). One option to provide a pre-fractured coal area to the caved zone is through the use of explosives (Amazo and Mishra 2019, Mondal and Roy 2019, Xie *et al.* 2016, Wojtecki L. *et al.* 2017). The use of permissible explosives to provide pre-fractured coal surrounding to the caved area is still a common practice in this type of operations.

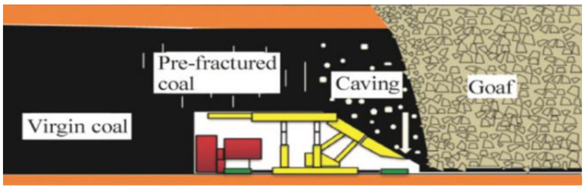

Fig. 1 LTCC model (Adapted from Xu (Xu, 2004))

It is documented how blasting techniques are used to pre-fracture the top and bottom of the coal seams and then allow the caving process (Konicek *et al.* 2013, Wojtecki *et al.* 2017, Sharma and Rai 2017). For this mining method, the optimization of the blasting energy to break the hard top and bottom zones of the coal is of importance (Silva *et al.* 2018, Saiang 2009).

This paper explores, using numerical analysis, the effects of decking in the blast-holes to pre-fracture the coal. The models compare the different fracture patterns generated when a concentrated charge is used in contrast to a combination of charges from two (2) to five (5) charges. To compare only the decking effects, the total amount of explosive per hole used in each model was kept the same. The detailed modeling process and the analysis of results are included in following sections.

2. Numerical model implementation

2.1 General considerations

The numerical model materials consist of explosives,

∗Corresponding author, Ph.D.
E-mail: feiliu182@163.com
∗∗Corresponding author, Professor
E-mail: slyang206@163.com

http://www.techno-press.org/?journal=gae&subpage=7
ISSN: 2005-307X (Print), 2092-6219 (Online)

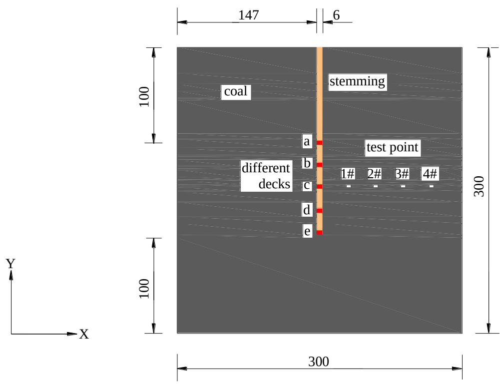

Fig. 2 Numerical model dimensions in centimeters

stemming material and coal. Due to the considerable dimensions of the mining opening compared to the diameter of the borehole and the thickness of the coal, the model was simplified into a plane strain conditions problem. Fig. 2 shows the geometry of the numerical models used in this paper. The coordinate system adopted is also shown in Fig. 2.

The total length of the concentrated explosive charge was 30 cm. Four measurement points were set at equal intervals in the middle horizontal position of the model to measure the propagation of stress waves in those locations.

The software used was ANSYS/LS-DYNA. This software is a well-known generic finite element software that can be used to analyze the nonlinear dynamic response of events. Using the Arbitrary Lagrangian-Eulerian (ALE) finite element analysis method, explosives can be defined as a fluid, and surrounding materials can be established as Lagrange units. Fluid-structure coupling is used to make connections between the two materials, so that substances can flow in the grid avoiding severe structural distortions of the elements. In this paper, the fluid-solid coupling algorithm is used to calculate the explosion effect of explosive on coal and the resultant crack propagation and distributions are analyzed. To facilitate modeling, a single-layer solid grid model was used with a free surface at the top of the model and non-reflected boundary at both sides and bottom of the model.

The location of the points where stress and strain data was collected from the models is shown in Fig. 2 (test points 1 to 4). According to the most popular explosion and detonation theories, the overpressure generated by the shock wave front is related to the amount of energy released initially that generates the shock wave.

Also, at some specific point, the overpressure will be a function of the distance source-point of interest (PI). The general relationship between the shock wave overpressure and the distance from the blast center can be given by (Greene *et al.* 2018).

$$\Delta \mathrm{P} = f\left(\frac{\sqrt[3]{\mathrm{q}}}{\mathrm{d}}\right) \tag{1}$$

where $\Delta \mathrm{P}$ is the overpressure on the shock wave front in MPa; d is the distance from the center of the explosion in meters, and q is the quantity of explosive in kg of TNT of explosive.

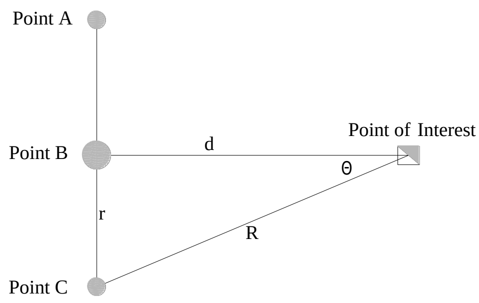

Fig. 3 Stress-strain points locations in the model

For example, the Engineer Technical Letter No. 1110-8-11, "Underwater blast monitoring" of the U.S. Army Corps of Engineers (Headquarters 1995), states that the approximate peak water shock pressure P, in imperial units from a detonation in free water is given by

$$\Delta P = 21{,}600(\lambda)^{-1.13} \tag{2}$$

where λ is the scaled range term $(\mathrm{d}/\sqrt[3]{\mathrm{q}})$.

For this paper, if a spherical charge of explosives is located at point B as shown in Fig. 3, the overpressure in the horizontal direction generated by the charge at the point of interest can be given by

$$P_{B-PI} = f\left(\frac{\sqrt[3]{q}}{r} \tan\theta\right) \tag{3}$$

where $r = d * \tan\theta$.

If, as mentioned before, plane strain conditions are adopted for the analysis and the concentrated explosive now is distributed by half to the locations of points A and C in Fig. 3, the horizontal component of the overpressure at the point of interest generated by the charges in Points A and C can be calculated as

$$P_{A\&C-PI} = f\left(\frac{\sqrt[3]{q/16}}{r} \sin 2\theta\right) \tag{4}$$

Eqs. (3) to (4) show that the horizontal component of the overpressure at the point of interest generated by the charge, or distributed charges, can be expressed as a function of the angle (θ) between one horizontal line and the location of charges in points A or C.

The use of Eqs. (3) to (4) require finding some specific constants for the medium (21,600 and -1.13 for water, Eq. (2) where the detonation is taking place. Finding such constants is beyond of the purpose of this paper. However, an analysis of the previous equations indicates that it is expected the generation of lower peak amplitudes in the stress generated for the decked charges than the concentrated charge, at the points of interest. This result is expected, although the detonation of the charges is done ideally in a simultaneous fashion and stress waves should arrive at the same time at the considered locations (constructive superposition of stress waves is expected).

2.2 Material properties in the model

2.2.1 Explosives

In this paper, the JWL equation of state was used to represent the material parameters of the explosive material. Lee and Kury (Lee *et al.* 1968) discussed the detonation velocity and pressure of various explosives and the results of accelerated metal experiments based on the adiabatic expansion equation of detonation products which is described by pressure, volume and energy (PVE). The equation of state relating the pressure and specific volume generated by the detonation process was given as Jones-Wilkens-Lee (JWL), combining the requirements of thermodynamics and fluid mechanics. It has been widely used in blasting calculations and can be written as follows.

$$P = A\left(1-\frac{\omega}{R_1 V}\right)e^{-R_1 V} + B\left(1-\frac{\omega}{R_2 V}\right)e^{-R_2 V} + \frac{\omega E_0}{V} \quad (5)$$

In Eq. (5), P is pressure in MPa. The variables R_1, R_2, and ω are parameters of the material. A and B are also parameters characteristic of the material, in GPa. E_0 is the initial specific internal energy in MJ. V is the relative volume.

For the numerical models in this paper, explosive material type emulsion was used. Jose (Jose *et al.* 2015) obtained the explosives specific JWL state parameters according to the test on emulsions and ANFO explosives by conducting copper column expansion measurements.

In this paper, the Titan-6000-E1 emulsion was used as the high-energy explosive. The parameters of the explosive are shown in the following tables (LSTC 2003).

Table 1 Material parameters of Titan-6000-E1 emulsion

Density/ρ_0 (Kg·m^{-3})	Detonation speed /D (m·s^{-1})	CJ Pressure/P_{CJ} (GPa)	CJ Relative volume/V_{CJ}	Ideal explosion heat/Q (KJ/Kg)
890	4688	374	7.33	4.15

Table 2 JWL state parameters of Titan-6000-E1 emulsion

A(GPa)	B(GPa)	C(GPa)	R_1	R_2	ω	E_0(GPa)
209.685	3.509	0.517	5.762	1.290	0.39	2.386

Table 3 Material parameters of coal

Density/ ρ_0 (Kg·m^{-3})	Elastic modulus/E (MPa)	Poisson's ratio	Yield stress (KN)	Tangent modulus (MPa)	Hardening coefficient	Failure strain
1860	2610	0.3	1.0	2.61	0.5	0.8

Table 4 Material parameters of stemming

Density/ρ_0 (g·cm^{-3})	Shear modulus/ G (GPa)	Bulk modulus/ K (GPa)	A_0	A_1	A_2	P_C(KN)	EPS_1	EPS_2
1.80	1.601E-4	1.328E+2	3.3E-3	1.31E-7	0.1232	0.0	0.0	0.05
EPS_3	EPS_4	EPS_5	EPS_6	EPS_7	EPS_8	EPS_9	EPS_{10}	P_1
0.09	0.11	0.15	0.19	0.21	0.22	0.25	0.30	0.0
P_2	P_3	P_4	P_5	P_6	P_7	P_8	P_9	P_{10}
3.42E-2	0.453	0.676	0.127	0.208	0.271	0.392	0.566	1.23

2.2.2 Coal and steaming

Coal has similar mechanical properties to rock. Researchers (Ganesh *et al.* 2015, Timo 2010, Houim and Oran 2015) have performed many numerical simulations on the mechanism of an explosion in rocks. Hao (Hao *et al.* 2002) programmed and linked an anisotropic continuum damage model to the available computer program Autodyn3D. As a result, the software has the capability to model rock mass behavior under blasting loads. The stress wave propagation and damage zone in the rock mass induced by underground explosions were simulated in such paper. Wang (Wang *et al.* 2007) implemented the Taylor–Chen–Kuszmaul (TCK) continuum damage model together with an erosion algorithm, into the explicit FE code of LS-DYNA, as a constitutive augmentation to analyze dynamic fracture behavior of rock in tension due to blast loading.

However, the literature shows few types of research on the propagation of the blasting wave and damage zone in coal as material. Wang (Wang *et al.* 1995) adopted the experimental method of super dynamic strain and flash X-ray photographing on the large coal sample to study the basic dynamic behavior of the propagation of the explosion stress wave, explosion energy conversion, and explosion cavity expansion of columnar explosive for hard coal. The effect of the pre-explosion of top coal was simulated and analyzed by using the finite element numerical calculation method.

The numerical models in ANSYS/LS-DYNA and implemented in this paper use some of the findings of previously mentioned researchers in coal as a material. The material properties of coal and stemming were implemented in the model following the procedures of the LS-DYNA keyword user's manual (LSTC 2003).

The constitutive behavior selected for coal was a type of Plastic-Kinematic, which is suited to model kinematic hardening plasticity with the option of including strain-rate effects (Wang 2019). The stemming was modeled as a von Misses type material using the keyword MAT_SOIL_AND_FOAM with elasto-plastic behavior. The parameters for the two materials are determined base on the two types mentioned above (and the references) and the in site coal of Jiangcang mine in western China as shown in Tables 3 to 4.

In Table 4, A_0~A_2 are yield function constant for plastic yield function, EPS_1~EPS_{10} are volumetric strain values (natural logarithmic values), and P_1~P_{10} are pressures corresponding to volumetric strain values, in KN.

As mentioned before, the objective of this paper is to analyze the effect of the distribution of explosives in a blast hole when various decks are used in comparison with a concentrated charge of explosive. The comparison between both conditions is measured through the fragmentation pattern in the coal seam, which is a fundamental factor for the coal caving mining technique.

2.3 Scenarios of analysis

As mentioned before, the main purpose of this paper is to analyze, using numerical models, the influence of decking in fragmentation of coal as part of the pre-fractured conditioning of the ground required in the LTCC mining method. This paper considers five scenarios. Such scenarios are included in Table 5.

In Table 5, to quantify the effect of the distribution of the explosive in the blast hole, a parameter called distribution parameter was used. The distribution parameter

Table 5 Distribution of explosive charges in the model

Scenario	Dispersed number	Charge location Point	Weight of each charge (g)	Distribution parameter D (%)
1	1	c	160.2	30.59
2	2	a, e	80.1	32.29
3	3	a, c, e	53.4	33.99
4	4	a, b, d, e	40.1	35.69
5	5	a, b, c, d, e	32.0	37.39

(D) in Table 5 is the ratio of the total surface area of the explosive to the total surface area of the blast hole which is calculated as

$$D = \frac{2\sum(l \times w + l \times t + w \times t)}{2(L \times W + L \times T + W \times T)} \quad (6)$$

where l, w and t are the length, width and thickness of each charge in cm, respectively; L, W and T are the length, width and thickness of the part of dispersed charges which is 100 cm, 6 cm and 1 cm, respectively.

This parameter was adopted as a metric to represent the distribution of the explosive in the blast hole. With the increase of the explosive distribution parameter (less explosive per charge), the explosives cannot be detonated due to the limitation of the critical diameter. The scenario number 5 corresponds to the maximum number of decks possible before the critical diameter effect.

The location of the charges is included in Fig. 2. The five scenarios were selected from a concentrated explosive charge (charge location at point c) to five different charges distributed the length of the blast hole.

In this paper, all models use the same amount of explosive in the blast hole, to analyze only the influence of the decking. In other words, the sum of charges in scenario 2 is equal to the concentrated charge of scenario 1. A similar analysis can be done for the other scenarios included in Table 5.

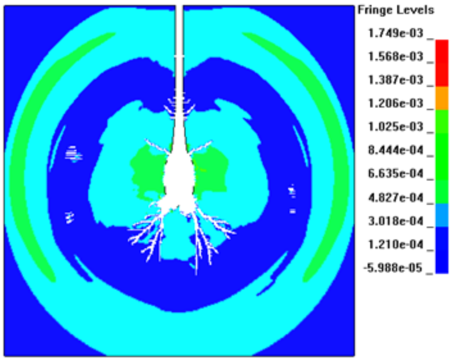

(a) t_1=1111 μs

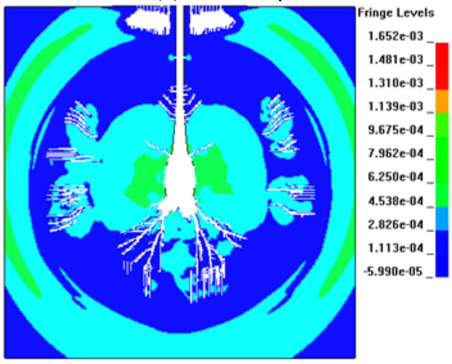

(b) t_2=1230 μs

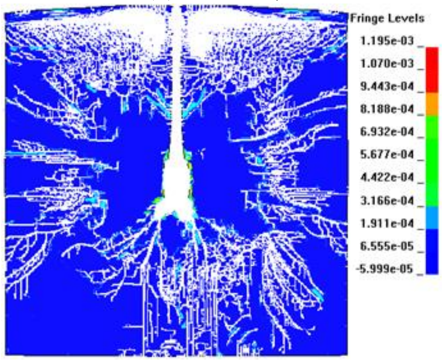

(c) t_3=2130 μs

Fig. 4 Explosion contours of stress obtained by concentrated explosive

3. Numerical models results

3.1 Concentrated charge results

Fig. 4 includes the results of the concentrated charge, equivalent to 160.2 g of explosive. Figs. 4(a)-4(b) show the stress conditions in the model for 1111 and 1230 microseconds after the explosion, respectively.

Fig. 4(c) shows that after 2130μs, the stress has been dissipated from the model, and the final fracture pattern is obtained. As shown in Figs. 4(a)-4(b), the cracks appeared around the blast hole at t_1=1111 μs and t_2=1230 μs in the zone of the explosive. This is due to the stress wave generated by the explosion impacting the wall of the blast hole and reaching the dynamic compressive strength of the coal, starting the initial crushing zone around the blast hole. The high-temperature and high-pressure gas generated by the explosion then enters the fractures, forming a stress concentration at the tip of the fracture, allowing the fracture to continue to expand forward. Some cracks appear in the coal after the explosion stress wave passed. At some areas of the model the stress wave does not break the coal for the stress at this present cannot cause neither the compress cracks nor the tensile and shear cracks. During the transmission process of the stress wave, an accumulation of elastic potential energy in the coal was observed. After the stress wave had passed, the elastic potential energy is released quickly, generating tension in the coal and producing more fractures.

At t_2=1230 μs, the stress wave reaches the top boundary of the model, and a reflected tensile wave is generated from that free surface of the model. Because the tensile strength of the coal is lower compared to its compressive strength, the top coal close to the upper boundary is fragmented from the tensile stress caused by the reflection of the stress wave (Fig. 4(b)).

While the previous process is occurring at the upper boundary of the model, at the same time in the near area of the blast hole, the coal is compressed and broken. The

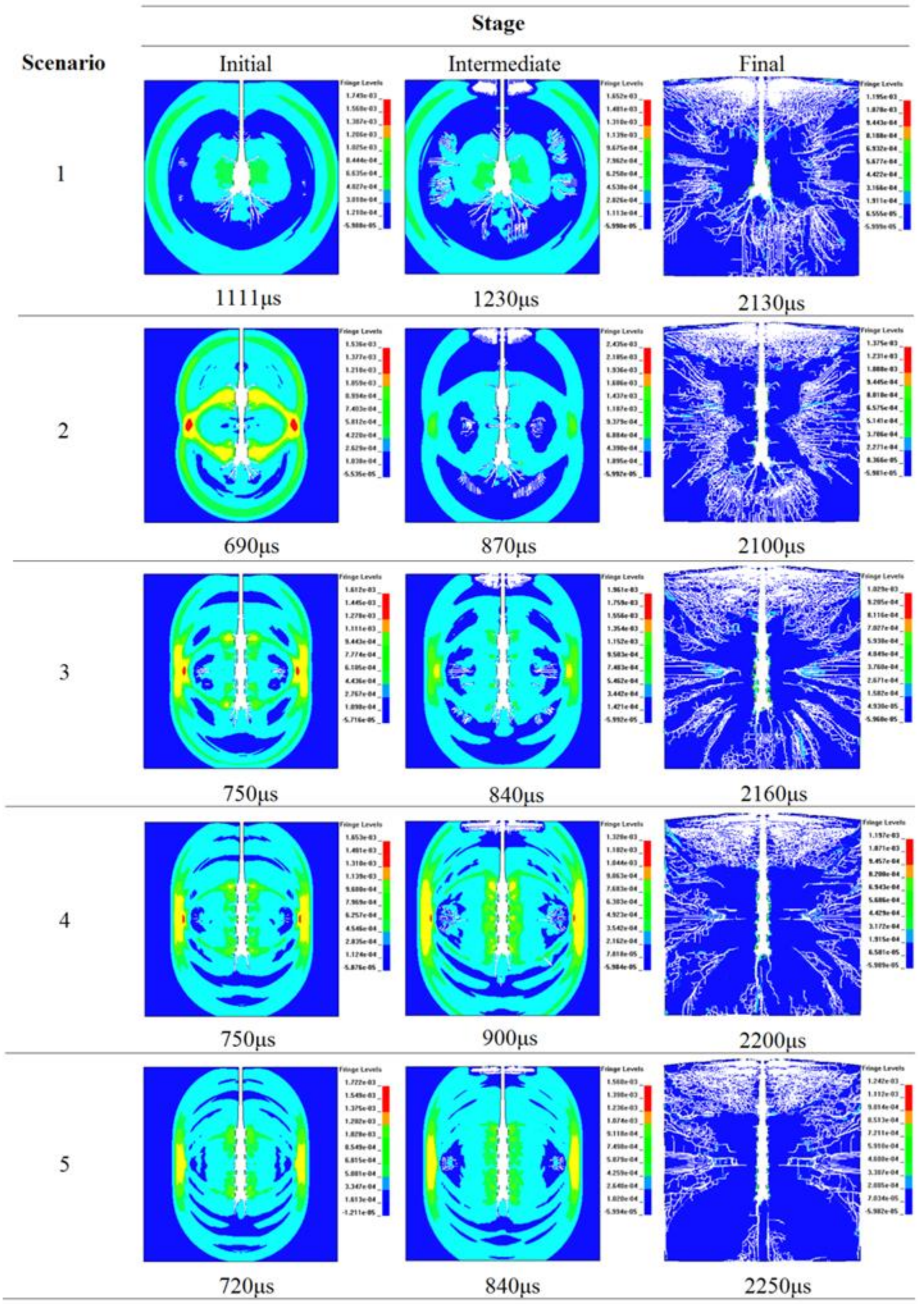

Fig. 5 Numerical models results for the five analyzed scenarios

explosion process is completed at t_3=2130μs. The coal is fully spalled at the top of the free surface. The final pattern of the cracks is developed radially with reference to the initial location of the explosive (Fig. 4(c)).

3.2 Other scenarios results

The previously described mechanisms were observed in the other numerical models. The main differences are the generation of a different number of stress waves according to the number of explosives charges in the blast hole. The results for the other scenarios are included in Fig. 5 for three conditions: a) Initial stage, b) stress reaching top reflective boundaries (intermediate stage) and c) fracture pattern totally developed (Final stage).

Table 6 Materials units and crushing degree

Scenario	Explosive units	Stemming units	Coal units	Death units	Crushing degree/%
1	180	810	89010	29766	33.44
2	180	1020	88800	33225	37.42
3	180	1020	88800	34467	38.81
4	192	1026	88782	26087	29.38
5	180	1032	88788	20095	22.63

As seen in Fig. 5, there is evidence of stress wave superposition at the mid location of the model in the scenarios 2 and 3. For scenarios 4 and 5, the superposition of waves occurs at other locations (see Fig. 5, first column). In the initial stage (first column) in Fig. 5, few fractures

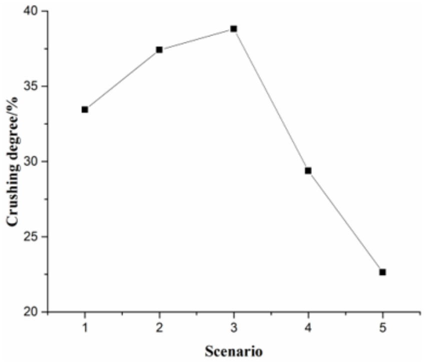

Fig. 6 Crushing degrees at different scenarios

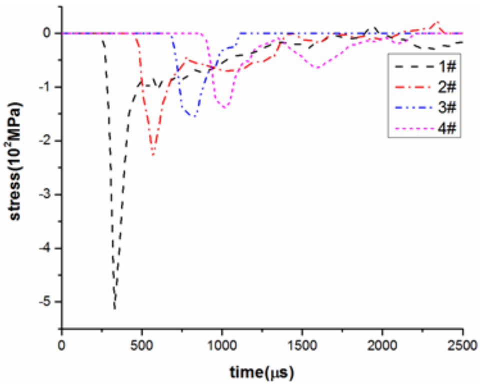

(a)

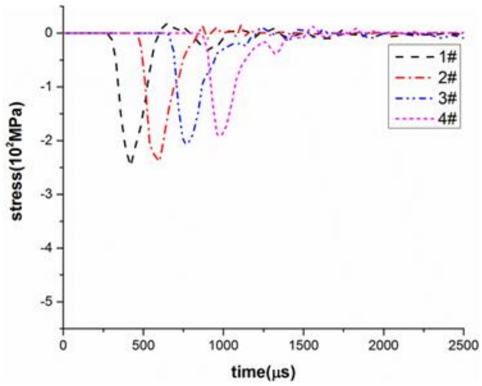

(b)

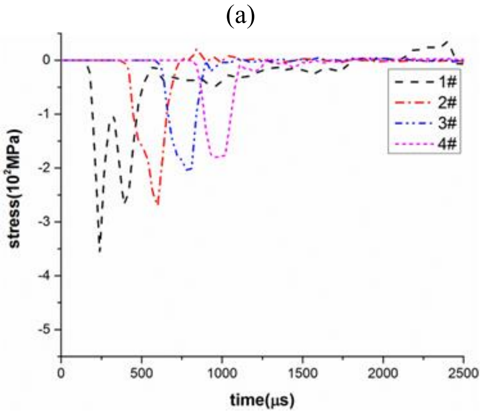

(c)

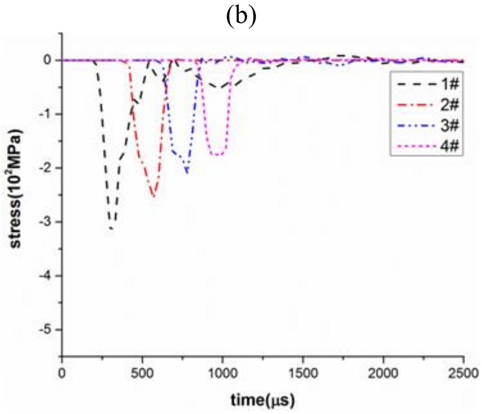

(d)

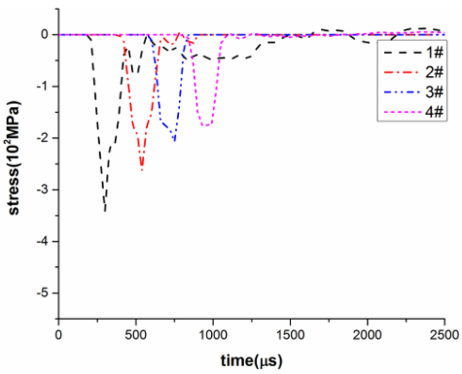

(e)

Fig. 7 Stress curves for the different scenarios

start to become evident and in the intermediate stage (second column) a clear initial development and pattern for the fractures is observed. In the intermediate stage within all the models, the stress wave arrived to the upper free boundary of the model and the reflection produced the spall effect in this boundary.

The last column in Fig. 5 shows the final stage of the models where all the stresses have dissipated and the final fracture pattern is observable. As seen in this column, the fracture pattern is directly related to the number of decks (or explosive charges) in the borehole. A visual inspection of Fig. 5 shows that scenario 3 presents a higher density of fractures in the numerical model (higher distribution of fractures in all the models) compared to other scenarios.

The number of the fractures can also be calculated by the 'death' units which mean that the units are overstressed and deleted. The crushing degree can be expressed by the ratio of the death units and the coal units. They can be calculated by using the LS-Prepostd in the ANSYS and are shown as follows.

As shown in the Table 6, different materials units are shown and the crushing degree is calculated. The relation between the crushing degree and different scenarios can be shown as follows.

As shown in Fig. 6, the crushing degree first increases and then decreases with the increase of the number of decks in the borehole. At scenario 3 (3 decks), the crushing degree reached the highest which is corresponding to the fracture pattern in Fig. 5.

3.3 Stress curves at points of interest

As mentioned before, four points were setup to collect the stress and strain curves from the numerical models. The locations of those points are included in Fig. 2. All the points are located in the middle part of the models. Fig. 7 shows the horizontal stress curves for each location and for each one of the numerical models (five in total).

Fig. 7 shows expected decay in the peak value of the horizontal stress with the increment of distance from the borehole. This is more evident for the scenario with a concentrated charge than the other scenarios. Figs. 7(b) to 7(e) show the reduction in the peak values due to the superposition of the stress waves when compared with the concentrated charge (Fig. 7(a)). This reduction agrees with the theoretical discussion presented in section 2.1 of this paper, where lower values were expected when stress generated by distributed charges are compared with a concentrated charge. This behavior was observed even though the explosives charges were detonated at the same time and constructive interference was expected in some form.

Two distinct wave peaks appeared in the stress waves by using three, four and five explosive charges. This is more evident for the location of points 1#, 2# and 3#. As the distance increases, the first peak attenuates and merges with the second peak.

Fig. 8 shows the peak values of the horizontal stress obtained by using different number of charges in the blast hole at different locations, for better understanding, the figure shows the absolute peak values of each stress waveform.

As mentioned before, with the increment of the distance from the test points to the explosive center, the peak value of stress shows a trend of reduction. As seen in Fig. 8, the decay is more pronounced for the concentrated charge.

Also, for this scenario, the peak of stress at the location

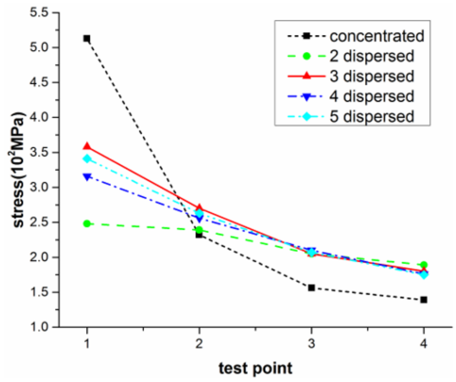

Fig. 8 Stress peak curves at each measured point

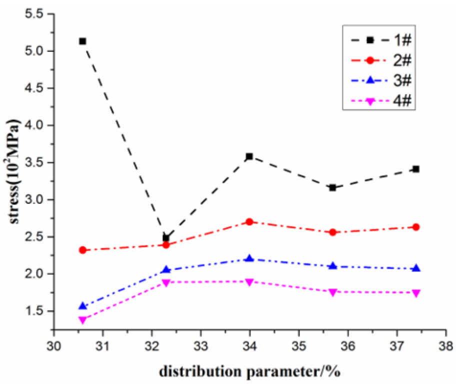

Fig. 9 Stress peak curves with the distribution of explosives

of point 1 is larger than the other scenarios. This behavior can be interpreted as the detonation of a concentrated explosive having a greater effect on the fracture of coal in the near zone of the blast hole and less effect at some distance. For scenarios different than the concentrated charge, the peak value of stress in the near area of the blast hole is significantly lower. As the distance increases, the peak of stress gradually decays and tends to be of the same value (scenarios 2 to 5). The trend in Fig. 8 for scenarios 2 to 5 shows that the different charge configurations have different fracture effects on the coal close to the blast hole, and they have similar fracture effects on the coal in far distances from the explosive charge.

When scenarios 2 to 5 are compared, scenario 3 shows stress peak values higher than the other scenarios. This agrees with the fracture pattern described before where scenario 3 shows a better fracture density distribution in the numerical model.

The effect of the increment in the distribution parameter, its relation with the absolute value of the horizontal stress peak and the point of interest is included in Fig. 9. In Fig. 9, lines 1, 2, 3 and 4 are for the measurement points 1, 2, 3 and 4 respectively.

In Fig. 9, the highest distribution parameter corresponds with the five explosives charges distributed in the blast hole while the lowest value represents the concentrated charge. As seen in Fig. 9, stresses at point 1 are always the highest. The explanation of scenario 3 being the most recommended to increase the fragmentation and fractures in the coal can be seen in Fig. 9. If Fig. 9 is analyzed in the range from 30.59% to 37.39%, for a value of 34.1% (corresponding to three explosives charges), all the curves show a maximum.

In other words, for the range under analysis, the horizontal stress peak values are the highest in all the points of interest at such value.

4. Conclusions

The explosion contours of stress were obtained by using explosion numerical simulation on coal as a rock-mass material. The calculation results were post-processed to obtain stress peak. The following conclusions can be obtained through comprehensive analysis.

(1) The explosion damage of coal is mainly caused by the tensile failure of the stress wave. The shock wave generated by the explosion strongly impacts the coal and resulting in impact crushing of the coal near the borehole wall. In the middle and far area, the coal is compressed and accumulates a large amount of elastic potential energy which is released rapidly causing tensile failures when the stress passes.

(2) The coal in the free surface of the top boundary is spalled for the reflection of explosion stress wave. The different scenarios results show that the three explosives charges present a higher density of fractures than others.

(3) The decay in the peak value of the horizontal stress with the increment of the distance from the borehole. As the dispersion of the explosive increases, two peaks of waves appeared in the stress wave, and the first wave gradually weakened and merged with the second wave crest. As the distance increases, the crest gradually becomes flat and horizontal. The stress wave peaks decay and eventually converge with horizontal distance.

(4) The scenario 3 with three explosives charges show stress peak values higher than others which are in agreement with the fracture pattern (more fractures in the model). The calculation of the materials units show that the crushing degree of the coal is corresponding to the fracture pattern.

(5) With the dispersion of explosive increase, a crest appeared obviously in the peak of stress wave. When the dispersion of the explosive is about 34.1%, that is, the three explosive charges were used, the peak value of stress reaches its maximum.

Acknowledgments

This research is supported by the National Natural Science Foundation of China (No.51674264, No.51574244) and National Key Research and Development Program of China (No.2017YFC0603002, No.2018YFC0604501).

References

Alehossein, H. and Poulsen, B.A. (2010), "Stress analysis of longwall top coal caving", *Int. J. Rock Mech. Min. Sci.*, **47**(1), 30-41. https://doi.org/10.1016/j.ijrmms.2009.07.004.

Azam, S. and Mishra, D.P. (2019), "Effects of particle size, dust concentration and dust-dispersion-air pressure on rock dust inertant requirement for coal dust explosion suppression in underground coal mines", *Proc. Safety Environ. Protect.* https://doi.org/10.1016/j.psep.2019.03.030.

Gasparotto, J., Chaves, P.R., Da Boit Martinello, K., da Rosa-Siva, H.T., Bortolin, R.C., Silva, L.F.O., Rabelo, T.K., da Silva, J., da Silva, F.R., Nordin, A.P., Soares, K., Borges, M.S., Gelain, D.P. and Moreira, J.C.F. (2018), "Obese rats are more vulnerable to inflammation, genotoxicity and oxidative stress induced by coal dust inhalation than non-obese rats", *Ecotoxicol. Environ. Safety*, **165**, 44-51. https://doi.org/10.1016/j.ecoenv.2018.08.097.

Greene, N.T., Alhussaini, M.A., Easter, J.R., Argo IV, T.F., Walilko, T. and Tollin, D.J. (2018), "Intracochlear pressure measurements during acoustic shock wave exposure", *Hear. Res.*, **365**, 149-164.

Hao, H. (2002), "Numerical analysis of blast-induced stress waves in a rock mass with anisotropic continuum damage models part 1: Equivalent material property approach", *Rock Mech. Rock Eng.*, **35**(2), 79-94.

Headquarters, U.S. Army Corps of Engineers (1995), "Underwater Blast Monitoring", Engineer Technical Letter No. 1110-8-11, U.S. Army Corps of Engineers, Washington, D.C., U.S.A.

Houim, R.W. and Oran, E.S. (2015), "Numerical simulation of dilute and dense layered coal-dust explosions", *Proc. Combust. Inst.*, **35**(2), 2083-2090. https://doi.org/10.1016/j.proci.2014.06.032.

Konicek, P., Soucek, K., Stas, L. and Singh, R. (2013), "Long-hole destress blasting for rockburst control during deep underground coal mining", *Int. J. Rock Mech. Min. Sci.*, **61**, 141-153. https://doi.org/10.1016/j.ijrmms.2013.02.001.

Le, T.D., Mitra, R., Oh, J. and Hebblewhite, B. (2017), "A review of cavability evaluation in longwall top coal caving", *Int. J. Min. Sci. Technol.*, **27**(6), 907-915. https://doi.org/10.1016/j.ijmst.2017.06.021.

Lee, E.L., Hornig, H.C. and Kury, J.W. (1968), "Adiabatic expansion of high explosive detonation products", Report UCRL-50422, University of California, Lawrence Radiation Laboratory, Livermore, California, U.S.A.

Li, N., Huang, B., Zhang, X., Yuyang, T. and Li, B. (2019), "Characteristics of microseismic waveforms induced by hydraulic fracturing in coal seam for coal rock dynamic disasters prevention", *Safe. Sci.*, **115**, 188-198. https://doi.org/10.1016/j.ssci.2019.01.024.

Livermore Software Technology Corporation (LSTC), (2003), *LS-DYNA Keyword User's Manual*, Version 970. Livermore, California, U.S.A.

Mondal, D. and Roy, P.N.S. (2019), "Fractal and seismic b-value study during dynamic roof displacements (roof fall and surface blasting) for enhancing safety in the longwall coal mines", *Eng. Geol.*, **253**,184-204. https://doi.org/10.1016/j.enggeo.2019.03.018.

Ozacar, V. (2018), "New methodology to prevent blasting damages for shallow tunnel", *Geomech. Eng.*, **15**(6), 1-12. https://doi.org/10.12989/gae.2018.15.6.001.

Saiang, D. (2009), "Stability analysis of the blast-induced damage zone by continuum and coupled continuum-discontinuum methods", *Eng. Geol.*, **116**, 1-11. https://doi.org/10.1016/j.enggeo.2009.07.011.

Sampath, K.H.S.M., Perera, M.S.A., Elsworth, D., Ranjith, P.G., Matthai, S.K., Rathnaweera, T. and Zhang, G. (2019), "Effect of coal maturity on CO2-based hydraulic fracturing process in coal seam gas reservoirs", *Fuel*, **236**, 179-189. https://doi.org/10.1016/j.fuel.2018.08.150.

Sanchidrián, J.A., Castedo, R., López, L.M. and Segarra, P. and Santos, A.P. (2015), "Determination of the JWL constants for ANFO and emulsion explosives from cylinder test data", *Cent. Eur. J. Energ. Mater.*, **12**(2), 177-194.

Sharma, S.K. and Rai, P. (2017), "Establishment of blasting design

parameters influencing mean fragment size using state-of-art statistical tools and techniques", *Measurement*, **96**, 34-51. https://doi.org/10.1016/j.measurement.2016.10.047.
Silva, J., Li, L. and Gernand, J.M. (2018), "Reliability analysis for mine blast performance based on delay type and firing time", *Int. J. Min. Sci. Technol.*, **28**(2), 195-204. https://doi.org/10.1016/j.ijmst.2017.07.004.
Thiagarajan, G., Kadambi, A.V., Robert, S. and Johnson, C.F. (2015), "Experimental and finite element analysis of doubly reinforced concrete slabs subjected to blast loads", *Int. J. Impact Eng.*, **75**, 162-173. https://doi.org/10.1016/j.ijimpeng.2014.07.018.
Timo, S. (2010), "Damage-viscoplastic consistency model with a parabolic cap for rocks with brittle and ductile behavior under low-velocity impact loading", *Int. J. Numer. Anal. Meth. Geomech.*, **34**, 1362-1386. https://doi.org/10.1002/nag.868.
Vakili, A. and Hebblewhite, B.K. (2010), "A new cavability assessment criterion for Longwall Top Coal Caving", *Int. J. Rock Mech. Min. Sci.*, **47**(8), 1317-1329. https://doi.org/10.1016/j.ijrmms.2010.08.010.
Wang, J.C., Liu, F. and Zhang, J.W. (2019), "Investigation on the propagation mechanism of explosion stress wave in underground mining", *Geomech. Eng.*, **17**(3), 295-305. https://doi.org/10.12989/gae.2019.17.3.295.
Wang, X.L. and Suo, Y.L. (1995), "Computer simulation of pre-explosion of fully mechanized coal caving roof in hard coal seam", *J. Xi'an. Min. Inst.*, **15**, 97-101.
Wang, Z.L. (2007), "Numerical simulation of tensile damage and blast crater in brittle rock due to underground explosion", *Int. J. Rock Mech. Min. Sci.*, **44**(5), 730-738. https://doi.org/10.1016/j.ijrmms.2006.11.004.
Wojtecki, L., Konicek, P. and Schreiber, J. (2017), "Effects of torpedo blasting on rockburst prevention during deep coal seam mining in the Upper Silesian Coal Basin", *J. Rock Mech. Geotech. Eng.*, **9**(4), 694-701. https://doi.org/10.1016/j.jrmge.2017.03.014.
Wojtecki, Ł., Konicek, P., Mendecki, M.J. and Zuberek, W.M. (2017), "Application of seismic parameters for estimation of destress blasting effectiveness", *Proc. Eng.*, **191**, 750-760. https://doi.org/10.1016/j.proeng.2017.05.241.
Xie, L.X., Lu, W.B. and Zhang, Q.B. (2016), "Damage evolution mechanisms of rock in deep tunnels induced by cut blasting", *Tunn. Undergr. Sp. Technol.*, **58**, 257-270. https://doi.org/10.1016/j.tust.2016.06.004.
Xu, B. (2004), "Application of the longwall top coal caving system in Australian thick seam coal mines", The University of New South Wales, Sydney, Australia.

CC